DESIGN AND STUDY OF BELT-TYPE CLAMPING AND PULLING DEVICE FOR POTATO STUBBLE
/
带式夹拔型马铃薯秧茬夹拔装置设计与试验

Guozeng GAN [1,2], Zhongcai WEI * [1 2 3], Guoliang SU [4], Zhen CUI [3], Chengqian JIN [1]
[1] School of Agricultural Engineering and Food Science, Shandong University of Technology, Zibo, 255091 / China;
[2] Institute of Modern Agricultural Equipment, Shandong University of Technology, Zibo / China;
[3] Shandong Wuzheng Group Co., Ltd., Rizhao / China;
[4] Shandong Star Agricultural Equipment Co., Ltd., Dezhou / China;
Tel: +86-18811126108; E-mail: weizc@sdut.edu.cn
DOI: https://doi.org/10.35633/inmateh-77-99

Keywords: *agricultural machinery, potato stubble, CPB, EDEM-RecurDyn*

ABSTRACT
To address problems such as frequent stubble entanglement and the heavy burden associated with separating potatoes from impurities during potato harvesting operations, a belt-type clamping and pulling device for potato stubble was developed to achieve complete stubble extraction. By analyzing the interaction between the stubble and the clamping and pulling belt (CPB), the causes of missed extraction and stubble breakage were identified, and the primary parameter ranges affecting extraction effectiveness were determined. An EDEM–RecurDyn coupled simulation model was established to investigate the stubble pulling process. Using the stubble breakage rate and stubble miss rate as evaluation indices, the main factors influencing pulling performance were identified as the forward speed of the device, the linear velocity of the CPB, and the ground clearance of the CPB. A three-factor, three-level orthogonal experiment was conducted, and quadratic regression models were developed with stubble breakage rate and stubble miss rate as response variables. Response surface analysis and parameter optimization were subsequently performed. The results indicate that at a device forward speed of 0.512 m/s, a CPB linear velocity of 1.08 m/s, and a CPB ground clearance of 50 mm, the stubble breakage rate and stubble miss rate were 6.45% and 8.73%, respectively. An experimental platform was constructed to validate the simulation results. Experimental tests showed that under the optimal parameter combination, the stubble miss rate was 7.5%, with a small relative error compared to the simulation results. These findings demonstrate that the proposed device meets the operational requirements for effective potato stubble pulling.

摘要
针对马铃薯收获机械在作业时易被秧茬缠绕和薯杂分离负担较重等问题,设计了一种带式夹拔型马铃薯秧茬夹拔装置实现秧茬的整根起拔.通过对秧茬与夹拔带之间的相互作用进行分析，确定了影响起拔效果参数的主要取值范围，阐明秧茬产生漏拔和拔断的原因。通过建立 EDEM-RecurDyn 耦合仿真模型，以机具前进速度、夹拔带转动线速度和夹拔带离地高度为试验因素，以秧茬漏拔率与拔断率为评价指标，进行三因素三水平正交试验，建立以秧茬拔断率与漏拔率为相应指标的二次回归模型，通过试验结果响应面分析与参数优化。结果表明，在机具前进速度 0.512m/s，夹拔带转速 1.08m/s，装置离地高度 50mm 时，秧茬拔断率 6.45%，漏拔率 8.73%。通过搭建试验平台，对仿真结果进行验证，试验表明在最佳参数组合下，秧茬漏拔率 7.5%，试验结果与仿真结果相对误差较小，装置满足马铃薯秧茬起拔作业设计要求。

INTRODUCTION
Potato tuber separation is a critical step in the mechanized harvesting of potatoes, but the challenge of balancing high efficiency with low damage has become the primary bottleneck hindering improvements in the efficiency and quality of mechanized potato harvesting in China *(Wang et al., 2023)*.

In order to remove crop residues, soil clods, and mixtures of the two, harvesting machinery requires larger material separation devices to ensure effective separation, resulting in bulkier harvesting machinery. However, the performance of mechanical harvesting and separation devices has significant limitations *(Dorokhov et al., 2022)*.

[1] *Guozeng, Gan, M.S. Stud. Eng; Zhongcai, Wei, Assoc. Prof. Ph.D. Eng.; Guoliang, Su, M.S. Stud. Eng; Zhen, Cui, Prof. Ph.D. Eng.; Chengqian, Jin, Prof. Ph.D. Eng.*

Currently, the potato stubble separation process is mainly characterized by low separation efficiency, a lack of low-loss, high-purity separation equipment, and the tendency of potato stubble to become entangled in key working parts of harvesting machinery *(Chen et al., 2019)*. In addition, the separation process during mechanical harvesting is incomplete, requiring secondary cleaning. These issues are hindering the development of high-end potato harvesting equipment *(Wei et al., 2019)*.

Currently, in China, scholars have established a relatively comprehensive research system in the field of potato stubble separation technology, with research covering multiple aspects such as separation mechanisms, device optimization, and process improvement *(Zhao et al., 2020)*. However, a significant research gap persists regarding the practical application of whole root pulling techniques for potato stubble. In China, the whole-root pulling approach has been primarily applied to field crop harvesting and agricultural stubble removal *(Yang et al., 2016; Wei et al., 2024)*. For instance, Hou J designed a floating clamping mechanism for garlic harvesting, which achieves auxiliary conveying and bulb slippage containment, thereby providing a novel approach for stable stem clamping *(Hou et al., 2023)*. Zou L designed a flexible clamping mechanism with variable stiffness characteristics using torsion springs and cam profiles, which reduces mechanical damage during the clamping of root and leaf vegetables, offering insights for low-damage clamping techniques *(Zou et al., 2021)*. Zhang J developed a cotton stalk harvesting method based on the belt clamping principle, featuring dual flexible belts for wrapping and pulling stalks *(Zhang et al., 2021)*. This approach effectively reduces the stalk breakage rate and provides a novel solution for intact stalk pulling. International scholars have established a relatively well-established theoretical system in clamping technology research, and these findings provide crucial support for technological development *(Heltoft et al., 2016)*. Lee J Y achieved stable gripping of geometrically complex objects through the design of an adaptive soft gripper, providing insights for multipurpose clamping device design *(Lee et al., 2020)*. Hachiya M implemented low-impact harvesting of cabbages using soft gripping tapes made of novel materials, offering guidance for flexible clamping device development *(Hachiy et al., 2004)*.

Inspired by the belt clamping principle and manual vine removal, this paper designs a device suitable for whole-plant pulling and removal of potato stubble before harvest. The device employs a flexible wrapping-clamping method combined with high-load-output pulling. The research findings can serve as a reference for developing low-damage, stable clamping and clearing equipment for stubble.

MATERIALS AND METHODS

Integrated structure and operating principle

The belt stubble pulling is engineered for whole root pulling of potato stubble, this device operates after the potato seedling killing. Removing potato stubble in advance can enhance the efficiency and quality of subsequent harvesting operations, while also helping to streamline the structure of the potato harvester and avoid over-complicated design, structure diagram of the belt-type clamping and pulling device is shown in Figure 1.

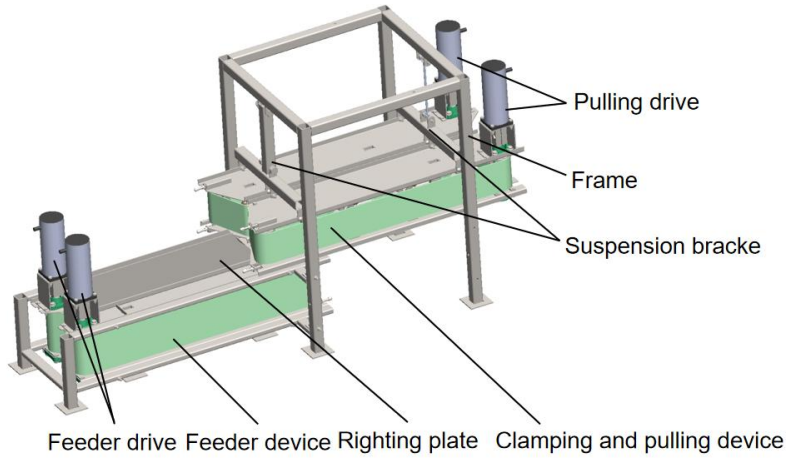

Fig. 1 – Structure diagram of the belt-type clamping and pulling device

During operation, the stubble feeder device is driven by the feeder drive, after stubble is manually fed into the device, the CPB guides and transports them rearward, simulating the forward movement of the device during field operation. The righting plate on both sides provide support to maintain the stubble in an upright position, as the stubble enters the pulling device, the pulling force generated by the backward movement of

the belt causes the stubble to tilt backward, when the stubble enters the pulling zone, the wave-shaped design of the CPB guides it to swing. This swinging motion simulates the manual stubble-pulling process, where gentle shaking reduces the resistance between the root system and the soil. Simultaneously, the clamping force exerted by the CPB on both sides significantly increases due to the tension provided by the spring tensioning device. This causes the potato stubble to undergo elastic deformation and be transported steadily backward under continuous clamping. This process simulates the mechanical behavior of the stubble being uprooted from the soil during field operation. Once fully uprooted from the soil, the potato stubble is conveyed by the CPB. It naturally disengages from the end of the conveyor belt and is deposited onto the ground in an orderly manner.

Key component design and parameter determination

The pulling device is the core component of the of the belt-type clamping and pulling device, as illustrated in Figure 2(a). After the potato stubble is fed into the pulling device, the pulling movement of the CPB can be divided into three phases, the clamping phase, the pulling phase, and the ejection phase, as shown in Figure 2(b).

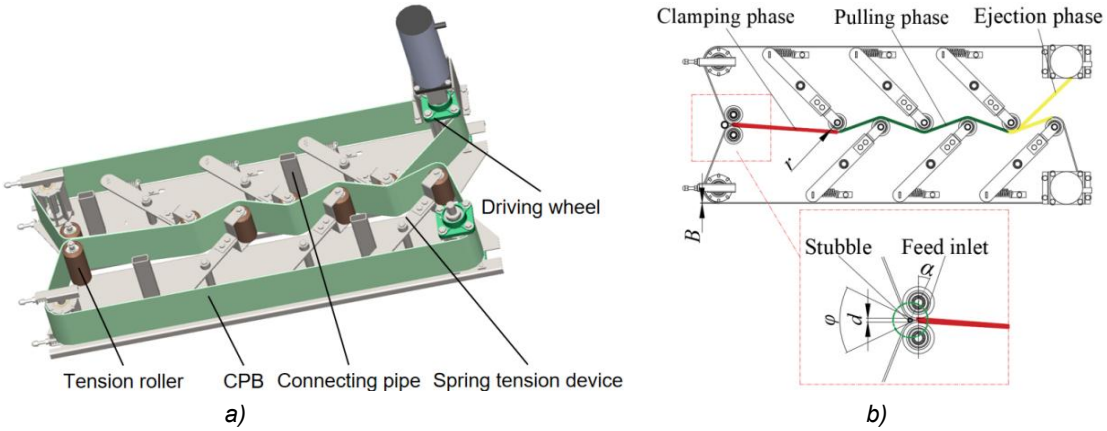

a) b)

Fig. 2 – Diagram of pulling device

B – thickness of the CPB; r - radius of the tension roller; φ - entry angle of the pulling device, (°); α - friction angle between the stubble and the CPB; d - diameter of the stubble, mm.

Analysis of the stubble feeding process

The stubble feeding phase constitutes a critical process node within the entire operational workflow, the device employs an adaptive V-flared inlet, with its physical structure depicted in Figure 3.

Fig. 3 – Physical diagram of the stubble inlet of the pulling device

To ensure smooth feeding of stubble, the entry angle *φ* of the clamping and pulling device and the friction angle *α* between the stubble and the CPB must satisfy *(Yao et al., 2023)*:

$$\arccos\frac{2r+2B}{2r+2B+d}=\varphi<2\alpha \tag{1}$$

where:

r is the tension roller radius, [mm]; B is the CPB thickness, [mm]; d is the stubble diameter, [mm].

Consulting literature on frictional properties of stubble *(Sun et al., 2021)*, the friction angle α between potato stubble and the CPB ranges approximately from 18° to 30°. Actual measurements show stubble diameter d varies from 8 mm to 12 mm. Considering operational requirements of the CPB and device stability, the CPB thickness B is set at 6 mm with tension roller radius r at 25 mm. The entry angle φ of the device is calculated to be 30°.

Analysis of the stubble clamping and pulling process

During the clamping stage, as the distance between two CPB gradually decreases, the force exerted on the stubble increases, causing them to tilt backward under the pull of the CPB. During the pulling phase, the normal-direction pressure applied by the CPB to the potato stubble abruptly increases under the action of the spring tensioning device, causing deformation in the clamped portion. As the CPB follows a sinusoidal path during this phase, an unclamped root region experiences transverse alternating forces *(He et al., 2018)*. This results in loosening between the potato stubble roots and the soil, thereby progressively diminishing the cohesive force binding the soil to the stubble. The separation of potato stubble from the soil requires overcoming both cohesive force and the stubble's own gravity. Given that the stubble's gravity is substantially smaller than the cohesive force, it can be considered negligible. The pulling force increases as the backward tilt angle of the stubble enlarges, while the cohesive force gradually diminishes under the stubble's oscillatory motion. When the pulling force exceeds the cohesive force, the stubble begins to detach from the soil *(Kaur et al., 2024)*. After a specific duration of applied force, complete separation between the stubble and soil is ultimately achieved. Following pulling from the soil, the potato stubble enters the ejection phase where it is propelled onto the ground by the CPB conveyor. A systematic analysis of cotton stalk processing demonstrates that the ejection phase exhibits no statistically significant impact coefficient on subsequent processing operations *(Zhang et al., 2021)*. Consequently, this study deliberately excludes the ejection-processing sequence from its scope to concentrate exclusively on core agronomic processes.

Impact of the spring tensioning device on the clamping and pulling process for potato stubble

The device uses a spring tensioning device that can adapt to changes in the diameter of the stubble, as illustrated in Figure 4(a). The spring tensioning devices are distributed in an alternating symmetrical configuration on both sides, with their spatial arrangement exhibiting uniform spacing. When stubble with larger stem diameters enter the device, the spring tensioning device rotates counterclockwise around the fixed shaft due to compression, the force analysis is shown in Figure 4(b).

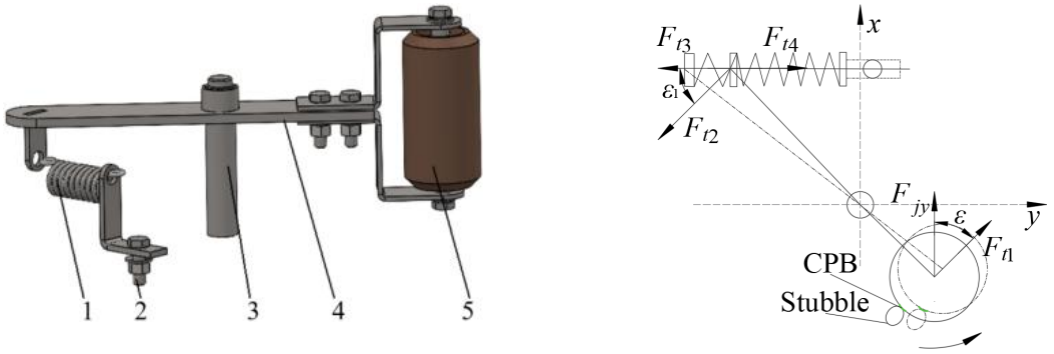

a) *b)*

Fig. 4 – Belt spring tensioning device

1 - Spring; 2 - Adjustment frame; 3 - Fixed shaft; 4 - Rotating arm; 5 - Tension roller

During the pulling process of stubble, the indirect force F_{jy} acting on the spring tensioning device satisfies:

$$\begin{cases} F_{t1} = F_{jy}\cos\varepsilon \\ \varepsilon + \varepsilon_1 = 90^\circ \\ F_{t2} = F_{t1} \\ F_{t3} = F_{t2}\cos\varepsilon_1 \\ F_{t3} = F_{t4} = kx \end{cases} \quad (2)$$

where: F_{jy} is the indirect force acting on the spring, [N]; F_{t1}-F_{t2} are the rotational force acting on the tension plate, [N]; ε is the tension angle, [°]; ε_1 is the angle of rotational force action, [°]; k is the spring stiffness coefficient, [N/m]; x is the horizontal extension distance of the spring, [m]; F_{t3} is the tension force acting on the spring, [N]; F_{t4} is the spring restoring force, [N].

The tension of the CPB increases, and consequently, the pulling force exerted on the stubble increases. The extension degree of the spring is positively correlated with the stubble thickness, serving as an uncontrollable variable. In contrast, the spring stiffness coefficient is a controllable variable that influences whether the stubble can smoothly enter and be completely uprooted, from Eq (2), can deduce that:

$$k = \frac{F_{jy}\sin(2\varepsilon)}{2x} \tag{3}$$

Based on existing research on the mechanical properties of potato stems, over 95% of mature potato stubble samples exhibit a pulling resistance within the range of 60 N to 200 N (*Xin et al., 2020*). To ensure stable operation of the device and effective clamping of the stubble, the tension angle ε is set within the range of 30° to 50°. The horizontal extension distance x of the spring correlates with the stubble stem diameter d, select the spring stiffness coefficient k of 5300 N/m.

Analysis of the stubble clamping and pulling phase

Initially, the stubble is subjected only to two fundamental forces in the vertical direction, its own gravity G and the soil support force. Upon entering the clamping and pulling device, the stubble is clamped by the CPB. After entering the clamping and pulling device, the stubble are subjected to pulling force F_N, and the root system and soil generate combined resistance, the lateral forces exerted by the soil on the stubble roots are F_{c1} and F'_{c1}. Analysis of the initial stress on stubble and soil when entering the device is illustrated in Fig. 5(a).

The pulling force and soil resistance satisfy:

$$\begin{cases} F_N = G + f + F_d + F_{Ty} \\ f = \mu_t (F_{c1} + F'_{c1}) \end{cases} \tag{4}$$

where: F_N is the pulling force applied to the stubble, [N]; G is the gravitational force acting on the stubble, [N]; f is the frictional resistance during relative motion between soil and stubble, [N]; F_d is the structural resistance of soil against pulling, [N]; F_{ty} is the adhesive force between soil and stubble, [N]; μ_t is the coefficient of friction between soil and stubble roots.

During the stubble pulling phase, the pulling force F_{N1} performs positive work, while the stubble's gravitational force G; the adhesive force F_{Ty1} exerted by soil on the roots perform negative work; the structural resistance F_{d1} against pulling applied by soil to the roots (*Chen et al., 2024*); the frictional force f_1 between soil and stubble, which is illustrated in Figure 5(b).

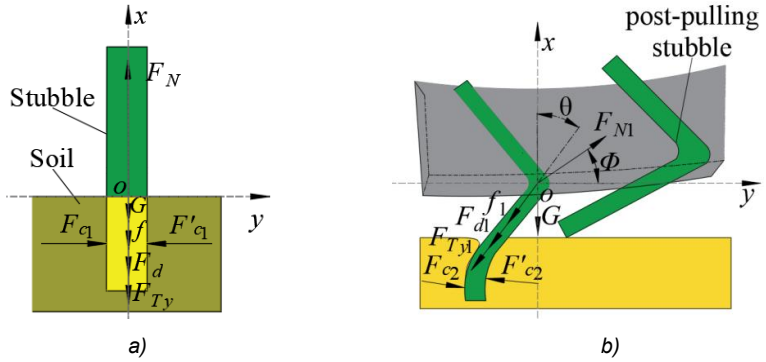

Fig. 5 – Schematic diagram of force analysis on stubble and soil

Effective disengagement of stubble from the soil is achieved only when the pulling force F_{N1} continuously performs work to overcome the composite soil resistance, this requires F_{N1} to satisfy:

$$F_{N1}\sin\Phi \geq (f_1 + F_{d1} + F_{Ty1})\cos\theta \tag{5}$$

During the pulling process, the stubble sways under the action of the CPB, which disrupts the integrity of the soil structure and leads to a continuous decrease in the combined soil–stubble resistance, thereby facilitating the extraction of the stubble. According to Equation (5), the extraction force angle Φ increases as the angle itself becomes larger, with Φ being determined by the operating speed of the belt-type pulling device and the ground clearance of the CPB. Given that the residual stubble height after vine killing is typically about 150 mm, the ground clearance of the CPB should be set below 100 mm to ensure effective clamping of the stubble. This prevents an insufficient clamping area from resulting in an excessively small pulling force F_{N1}. Furthermore, taking into account the surface unevenness of the potato ridges and to avoid collision between the device and the soil, the ground clearance of the CPB should be maintained above 30 mm.

Influence of wave profile geometric parameters of the CPB on stubble harvesting effectiveness

The device innovatively adopts a wavy CPB structure design, which increases the clamping contact area to enhance clamping stability and adaptability to the diverse shapes of stubble. Under the constraint of the tensioning roller, the CPB follows a sinusoidal wave trajectory. As the stubble enter the pulling zone, they oscillate under the action of the wavy CPB, as shown in Figure 6(a), the physical diagram is shown in Figure 6(b).

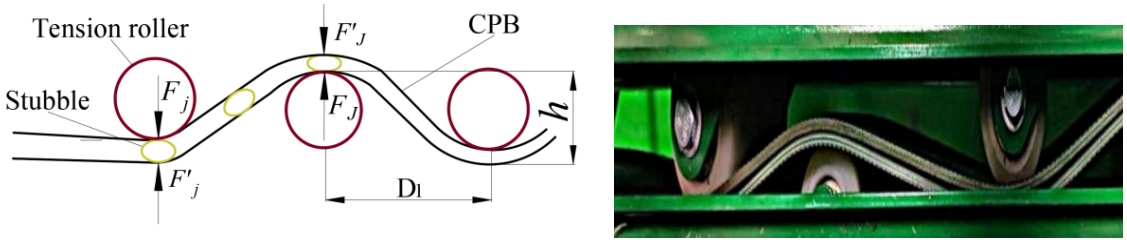

a) b)

Fig. 6 – Analysis diagram of stubble residues during pulling phase

To ensure effective stubble extraction and operational efficiency, three spring tensioning devices are symmetrically arranged on both sides along the working direction. The undulating profile of the CPB is defined by its wave height and wavelength. This profile shows a negative correlation with the combined soil–stubble resistance and significantly affects the success of stubble pulling *(Dirr et al., 2023)*. In potato cultivation, typical plant spacing ranges from 200 mm to 350 mm. Based on anti-clogging design requirements, the spacing between tensioning rollers, D_1, is set to 150 mm. The wave height *h* of the belt is positively correlated with the tensioning angle ε of the spring tensioning device. Accordingly, the calculated range for the wave height h is determined to be 140 mm to 220 mm.

Influence of device travel speed and CPB operational speed on stubble harvesting effectiveness

When the stubble initially contacts the belt, the clamped portion of the stubble undergoes approximately linear motion, after the stubble enters the pulling phase, its trajectory deviates from a straight line due to the guiding effect of the wave profile of the CPB, exhibiting an overall cycloid-like characteristic. If the driving wheel speed is excessively high, the overly brief pulling duration can cause a surge in dynamic loads on the CPB, potentially leading to stubble fracture. Conversely, if the driving wheel speed is too low, the prolonged pulling time not only reduces operational efficiency but may also cause blockages due to stubble retention.

During the pulling process, the stubble is extracted from the soil when the applied pulling force F_{N2} exceeds the combined soil resistance. When the mechanical work done by the CPB and tension roller system on the stubble reaches or exceeds the minimum work required for the stubble to detach from the soil, effective stubble removal can be achieved, this process can be expressed as:

$$\int_{t_0}^{t_0+t_1} F_{N1}\sin\Phi w r_q \mathrm{d}t \geq \int_0^{h_y} (f_1 + F_{d1} + F_{T1})\cos\theta \mathrm{d}x \tag{6}$$

where:

t_0 is the time instant when stubble pulling begins, [s]; t_1 is the time required for complete stubble pulling, [s]; w is the angular velocity of the driving wheel, [rad/s]; R is the radius of driving wheel, [mm]; h_y is the extracted length of the stubble, [mm].

Equation (6) indicates that the key factor for successful stubble pulling lies in the magnitude of work done by the pulling force on the stubble. This work primarily depends on both the pulling time and the pulling force magnitude, where the pulling time is inversely proportional to the device's forward speed. During the stubble pulling phase, the forward speed of the device v_m should be less than the linear velocity of the belt v_c, the linear velocity of the CPB is expressed as:

$$v_c = \frac{120\pi R n}{10^6} \tag{7}$$

where:

n is the rotational speed of the driving wheel, [r/min].

To ensure both operational efficiency and effectiveness of the device, the clamping and pulling mechanism is designed to simultaneously handle 2 to 3 stubble plants. With reference to the acceptable miss rates in cotton stubble harvesting, the pulling time per individual stubble should be maintained between 1.2 s and 3 s. Given that the combined length of the clamping and pulling phases is approximately 1 m, the required travel speed of the device falls within the range of 0.33 m/s to 0.83 m/s. Considering a driving wheel radius R of 40 mm, the operating linear velocity of the CPB is accordingly selected between 1.0 m/s and 1.2 m/s. This range ensures successful stubble extraction while meeting the constraint of minimum effective action time.

Analysis of missed stubble pulling

Missed stubble pulling is a typical failure mode in mechanized potato harvesting operations. Maintaining the stubble miss rate within a reasonable range is therefore essential to ensure the stable and efficient performance of subsequent field operations. The occurrence of missed pulling is primarily influenced by two factors.

Firstly, severe lodging of some potato stubble results in an insufficient clamped length, preventing the generation of adequate pulling force and leading to pulling failure. Secondly, extreme soil conditions significantly enhance the adhesion between stubble and soil *(Oshunsanya, 2016)*, resulting in excessive pull-out strength insufficient pulling force causes relative slippage between the stubble and the CPB *(Wang et al., 2021)*. Analysis reveals that the tension force F_z provided by the CPB reaches its maximum when the stubble is positioned at two characteristic phases, the trough and the peak of the CPB's undulation, as illustrated in Figure 7.

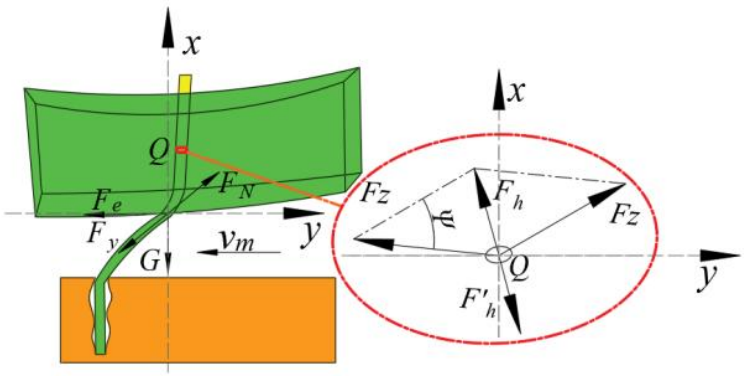

Fig. 7 – Mechanical force analysis diagram of stubble

where:

Q is the centers of the stubble; F_h is the compressive force on the stubble, [N]; F_z is the tension force in the CPB, [N]; Ψ is the clamping angles of the CPB, [°]; F_y is the composite soil and stubble resistance, [N]; F_e is the thrust force exerted on the stubble by the device's forward motion, [N].

The stubble miss rate can be reduced by increasing the pulling force F_N or reducing the composite resistance F_y between the soil and the stubble. The composite resistance F_y gradually decreases due to the swaying of the stubble. The pulling force F_N can be increased by increasing the squeezing force F_J of CPB on the stubble, perform a stress analysis on the cross-section of the stubble, measured weight m of the potato stubble after vine killing ranged approximately from 40 g to 100 g, according to the formula for centripetal force, the centripetal force F_x of the stubble is:

$$F_x = \frac{mv_c^2}{r} \tag{8}$$

The force F_h exerted on the stubble by the tension of the CPB is given by:

$$F_h = 2F_z \sin\frac{\Psi}{2} \tag{9}$$

The force F_J exerted by the CPB on the stubble is defined as:

$$F_J = F_x + F_h = 2F_z \sin\frac{\Psi}{2} + \frac{mv_c^2}{r} \tag{10}$$

Based on Equation (10), an increase in the CPB's speed linearly increases the squeezing force applied to the stubble. However, an excessively high linear velocity raises the risk of stubble breakage due to excessive dynamic loads. Conversely, an insufficiently low linear velocity can compromise stable clamping by the CPB, leading to slip-off during pulling and resulting in missed extraction.

Analysis of stubble breakage

Stubble breakage reduces the efficiency of subsequent cleaning operations and compromises potato harvesting quality. Preliminary tests revealed that the breakage of stubble exhibits significant spatial concentration, with breakage primarily occurring in the transition zone between the clamped portion of the stubble and the root *(Khamaletdinov et al., 2020)*. This region exhibits significant stress concentration, this region experiences pronounced stress concentration, manifesting primarily as transverse and oblique fracture modes. Analysis reveals that a positive correlation between the stubble breakage rate and deformation magnitude, the schematic diagram of stubble deformation is shown in Figure 8.

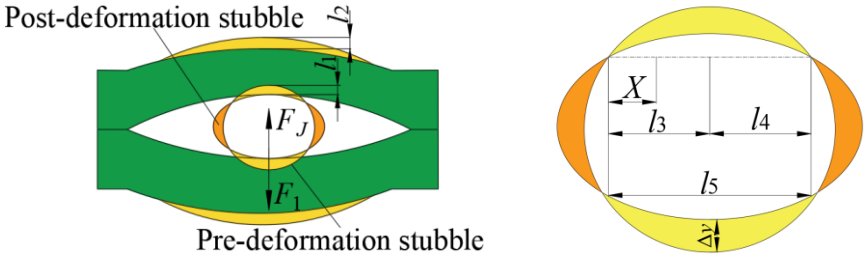

Fig. 8 – Deformation characteristics of stubble

where:

F_1 is the deformation resistance generated by the stubble, [N]; l_1 is the deformation of the stubble, [mm]; l_2 is the deformation of the belt, [mm]; l_3-l_4 are the length of the deformed section of the stubble, [mm]; l_5 is the total deformation length of stubble, [mm]; Δy is the deflection of stubble deformation.

The bending moment M acting on the stubble stem can be expressed as:

$$M = \frac{F_J l_4}{l_5} X - F_J (X - l_3) \tag{11}$$

The bending moments on both sides of the stubble are equal, integrating over one segment of the stem yields:

$$MJ \frac{\mathrm{d}^2 y}{\mathrm{d}x^2} = \frac{F_J l_3}{l_4} \tag{12}$$

where: J is the rotational inertia of the stubble.

The stem deformation deflection Δy can be expressed as:

$$\Delta y = \frac{F_J l_3 l_4 (l_5 - l_4)}{6MJ} \tag{13}$$

The stress experienced by the stubble demonstrates a proportional relationship with deformation deflection. A reduction in deformation deflection leads to a significant decrease in induced stress. Equation 13 indicates that deformation deflection is correlated with the elastic modulus, which itself exhibits a positive correlation with the contact area of the stubble stem. Therefore, the use of an undulating flexible belt effectively minimizes stubble deformation through belt compliance. This mitigation helps reduce internal structural damage and lowers the stubble breakage rate.

RecurDyn-EDEM coupled simulation

To accurately simulate the interaction between the device and the stubble, this paper uses a coupled simulation using RecurDyn and EDEM software to dynamically simulate the stubble pulling process, thereby verifying the optimal operating parameters.

To accurately represent the movement and force variations of stubble during the clamping and pulling process, a flexible stubble model was created using a multi-ball aggregation method. Five stubble plants were continuously positioned along the machine's forward direction, spaced 250 mm apart. Each stubble stem had a diameter of 10 mm, with 150 mm of stubble remaining on the ridge. The root depth was set at 60 mm. The stubble model was filled using internally generated single-ball particles with a radius of 1 mm and integrated via cohesive bonds. After completing the stubble generation, a virtual soil trench with dimensions (L×W×H) of 1300 mm×400 mm×100 mm was established, the discrete element model is shown in Fig. 9. It was filled using a 2 mm radius single-sphere particle gravity fall method and assembled using cohesive bonds *(Wang et al., 2025)*. Sandy loam was selected as the soil type, the Poisson's ratio, density, and shear modulus of the stubble residue were 0.28, 999 kg/m³, and 3.35×10⁶ Pa, respectively. The soil's Poisson's ratio, density, and shear modulus were 0.25, 2500 kg/m³, and 1×10⁸ Pa. The contact parameters and cohesion parameters related to the discrete element model are shown in Table 1.

Table 1

Discrete element model parameters

Parameter	Value
Soil-soil restitution coefficient	0.56
Soil-soil static friction coefficient	0.31

Parameter	Value
Soil-soil dynamic friction coefficient	0.13
Soil-stubble restitution coefficient	0.12
Soil-stubble static friction coefficient	0.43
Soil-stubble dynamic friction coefficient	0.01
Stubble-stubble restitution coefficient	0.8
Stubble-stubble static friction coefficient	0.8
Stubble-stubble dynamic friction coefficient	0.8
Stubble-rubber restitution coefficient	0.56
Stubble-rubber static friction coefficient	0.53
Stubble-rubber dynamic friction coefficient	0.42
Polyurethane-rubber restitution coefficient	0.5
Polyurethane-rubber static friction coefficient	0.68
Polyurethane-rubber dynamic friction coefficient	0.58
Stubble-stubble unit area normal stiffness/(N/m^3)	7.5×10^9
Stubble-stubble unit area tangential stiffness/(N/m^3)	5.6×10^8
Stubble-stubble critical normal stress/(Pa)	6×10^7
Stubble-stubble critical tangential stress/(Pa)	7×10^6
Stubble-stubble bonding radius/(mm)	2
Soil-soil Unit area normal stiffness/(N/m^3)	2.5×10^6
Soil-soil Unit area tangential stiffness/(N/m^3)	1.5×10^6
Soil-soil critical normal stress/(Pa)	25000
Soil-soil critical tangential stress/(Pa)	15000
Soil-soil bonding radius/(mm)	4.2

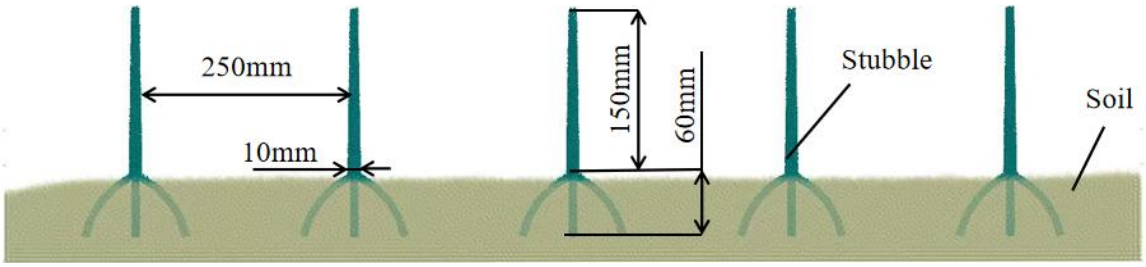

Fig. 9 – Discrete element model

To improve simulation speed, the device was simplified by retaining only the CPB that contacts the stubble under actual operating conditions. Due to limitations of the EDEM software in accurately configuring complex motions, the CPB were modeled using the Toolkit-Belt module in RecurDyn to better simulate the real operational behavior of the CPB, the CPB materials utilize rubber. All roller materials are selected from polyurethane, the driving and driven rollers have a diameter of 80 mm, while the tension roller has a diameter of 50 mm; all three are 120 mm in height.

Based on the previous analysis, the pulling force required to remove seedling stubbles ranges from approximately 60 N to 200 N, and the clamping force applied by the belt must reach about 400 N. Given that the coefficient of friction between the seedling stubble and the clamping belt is approximately 0.53, Equation (10) indicates that a belt tension of 525 N will ensure effective clamping and pulling of the stubble. To achieve a closed, wave shaped CPB, the belts were initially constructed as shell belts. Motion joints were then added to the tension rollers on both sides for simulation.

By horizontally moving the two tension rollers, the belt was tensioned and closed into a wave profile. After the belt reached full contact closure, the model was exported using the Extract function.

Following belt construction, the Patch function in FFlex Edit was applied to soften the belt. After exporting the model, the External SPI module in RecurDyn was used to identify all geometric bodies interacting with the clamped stubble segment model and to generate a Wall file. This file was then imported into EDEM via the "Import Geometry… from RecurDyn" function. The coupling interface between EDEM and RecurDyn was activated, and a coupled simulation analysis was performed. The coupled simulation model of the stubble clamping and pulling system is shown in Figure 10.

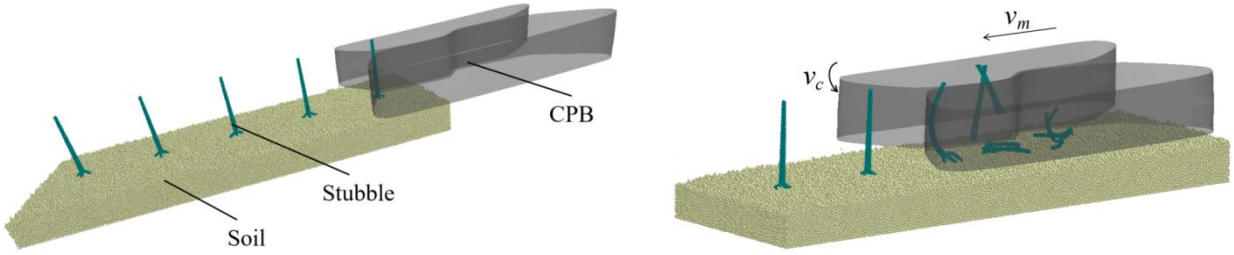

Fig. 10 – Coupled simulation test model

Coupled simulation tests and results

Selection of simulation input parameters and evaluation indicators

Based on theoretical analysis, the device forward speed X_1, the linear velocity of the CPB X_2, and the ground clearance of the CPB X_3 were selected as the simulation input parameters. Preliminary simulation tests revealed that an excessively high forward speed substantially increased stubble breakage rate, while an excessively low speed prolonged the time required to collect all stubble, thereby reducing efficiency. Considering that device forward speed X_1 should remain below the 3.5 km/h operational speed typical of potato haulm destroyers, the X_1 parameter was set within a range of 0.4~0.8 m/s. Drawing on theoretical analysis of the optimal working conditions for the pulling device, the X_2 parameter was defined within 1.0~1.2 m/s, and the X_3 parameter within 30~70 mm. A three-factor, three-level Box-Behnken orthogonal experimental design was adopted, with the factor coding presented in Table 2.

Table 2

Coding of test factors

Codes	Factors		
	Forward speed of the device X_1 / m·s^{-1})	Linear velocity of CPB X_2 / m·s^{-1}	Ground clearance of CPB X_3 / mm
-1	0.4	1.0	30
0	0.6	1.1	50
1	0.8	1.2	70

To validate the effectiveness of the belt-type clamping and pulling device for potato stubble, evaluation metrics were adapted from cotton stalk extraction tests, stubble miss rate Y_1 and stubble breakage rate Y_2 is selected as performance evaluation indicators for the belt-type clamping and pulling device for potato stubble, their calculation equations are as follows:

$$\begin{cases} Y_1 = \dfrac{P_{L1}}{P_Z} \times 100\% \\ Y_2 = \dfrac{P_{L2}}{P_Z} \times 100\% \end{cases} \quad (14)$$

where:

P_{L1} is the number of miss stubble per group; P_{L2} is the number of breakage stubble per group; P_Z is the total stubble count per group.

RESULTS

Test results and analysis of variance

The three-factor, three-level orthogonal test method was adopted, with the X_1, X_2 and X_3 as the test factors, and the Y_1 and Y_2 as the evaluation indexes. A total of 17 groups of combination tests were carried out. The experimental scheme and results are shown in Table 3.

Table 3

Experimental scheme and results

No.	Factors			Stubble miss rate Y1/%	Stubble breakage rate Y2/%
	X1	X2	X3		
1	0	0	0	8.11	7.56
2	0	1	-1	9.45	9.33
3	0	-1	1	9.34	8.89
4	0	0	0	8.67	7.11
5	-1	0	-1	8.93	6.22
6	-1	0	1	10.51	11.56
7	1	1	0	11.26	14.22
8	1	0	1	10.94	12.44
9	0	0	0	8.72	8.44
10	-1	-1	0	9.45	8.89
11	0	0	0	8.36	6.67
12	0	-1	-1	7.24	9.33
13	-1	1	0	10.26	10.22
14	1	-1	0	9.38	10.22
15	1	0	-1	9.76	9.78
16	0	1	1	11.07	13.33
17	0	0	0	8.36	7.56

The test results were processed using Design-Expert software to obtain the quadratic polynomial regression equations of Y_1 and Y_2, and analyzed by variance and significance test. The variance analysis of the stubble miss rate is shown in Table 4. From the table, it can be seen that the model has a highly significant fit. X_2, X_3, and X_1^2 have a highly significant effect on the stubble miss rate, while X_1, X_2^2, and X_3^2 have a relatively significant effect on the stubble miss rate. The remaining items have no significant effect.

Table 4

Variance analysis on the stubble miss rate

Index	Source of variance	Sum of square	Freedom	F value	P value
Y_1	**Model**	19.86	9	26.77	0.0001
	X_1	0.5995	1	7.27	0.0308
	X_2	5.49	1	66.65	<0.0001
	X_3	5.25	1	66.67	<0.0001
	X_1X_2	0.2862	1	3.47	0.1047
	X_1X_3	0.04	1	0.4852	0.5085
	X_2X_3	0.0576	1	0.6987	0.4308
	X_1^2	6.08	1	73.77	<0.0001
	X_2^2	0.8217	1	9.97	0.0160
	X_3^2	0.6380	1	7.74	0.0272
	Residual	0.5770	7		
	Lack of fit	0.3241	3	1.71	0.3023
	Pure error	0.2529	4		
	Cor total	20.44	16		

The variance analysis of the stubble breakage rate is shown in Table 5, where X_1, X_2, X_3, X_1^2, and X_2^2 have a highly significant effect on the stubble breakage rate, X_2X_3 and X_3^2 have a relatively significant effect on the stubble breakage rate, and the remaining items have no significant effect.

Table 5

Variance analysis on the stubble breakage rate

Index	Source of variance	Sum of square	Freedom	F value	P value
Y_2	**Model**	80.49	9	14.26	0.0010
	X_1	11.93	1	19.03	0.0033
	X_2	11.93	1	19.03	0.0033
	X_3	16.70	1	26.64	0.0013
	X_1X_2	1.78	1	2.84	0.1357

Index	Source of variance	Sum of square	Freedom	F value	P value
	X_1X_3	1.80	1	2.86	0.1344
	X_2X_3	4.93	1	7.86	0.0264
	X_1^2	10.78	1	17.19	0.0043
	X_2^2	13.94	1	22.24	0.0022
	X_3^2	3.66	1	5.84	0.0464
	Residual	4.39	7		
	Lack of fit	2.66	3	2.06	0.2488
	Pure error	1.73	4		
	Cor total	84.88	16		

Response surface analysis

The response surfaces of the parameter combinations with significant effects on the evaluation indicators are shown in Fig. 11. As shown in Figures 11a and 11d, with the ground clearance and forward speed held constant, an increase in the CPB's linear velocity X_2 enhances the dynamic pulling force transmitted to the stubble. Mechanistically, the higher velocity increases the applied impulse, which raises the stubble miss rate Y_1 as some stubbles are pulled through rapidly without being fully clamped. Concurrently, the stubble breakage rate Y_2 declines because the increased kinetic energy promotes cleaner fracture at weaker sections. Theoretically, beyond a certain point, the pulling force approaches a critical threshold while its duration shortens, leading to a transition where both Y_1 and Y_2 exhibit a non-monotonic trend—initially decreasing before rising.

In Figures 11b and 11e, under fixed ground clearance, an increase in forward speed X_1 alters the force distribution along the stubble. The resultant increase in longitudinal loading elevates Y_1 due to accelerated dislodgement, while Y_2 decreases as the stress concentrates near the root. However, further increase in X_1 reduces the interaction time between the CPB and the stubble, weakening the effective transfer of pulling energy and thus causing Y_1 to fall and Y_2 to rise.

As illustrated in Figures 11c and 11f, with CPB linear velocity and forward speed constant, increasing the ground clearance X_3 modifies the clamping geometry and mechanical advantage. Initially, the vertical force component increases, elevating Y_1 and reducing Y_2. Beyond an optimum clearance, however, the reduced contact area and compromised grip diminish the extraction force, resulting in a drop in Y_1 and a pronounced rise in Y_2 due to incomplete pulling and increased structural failure.

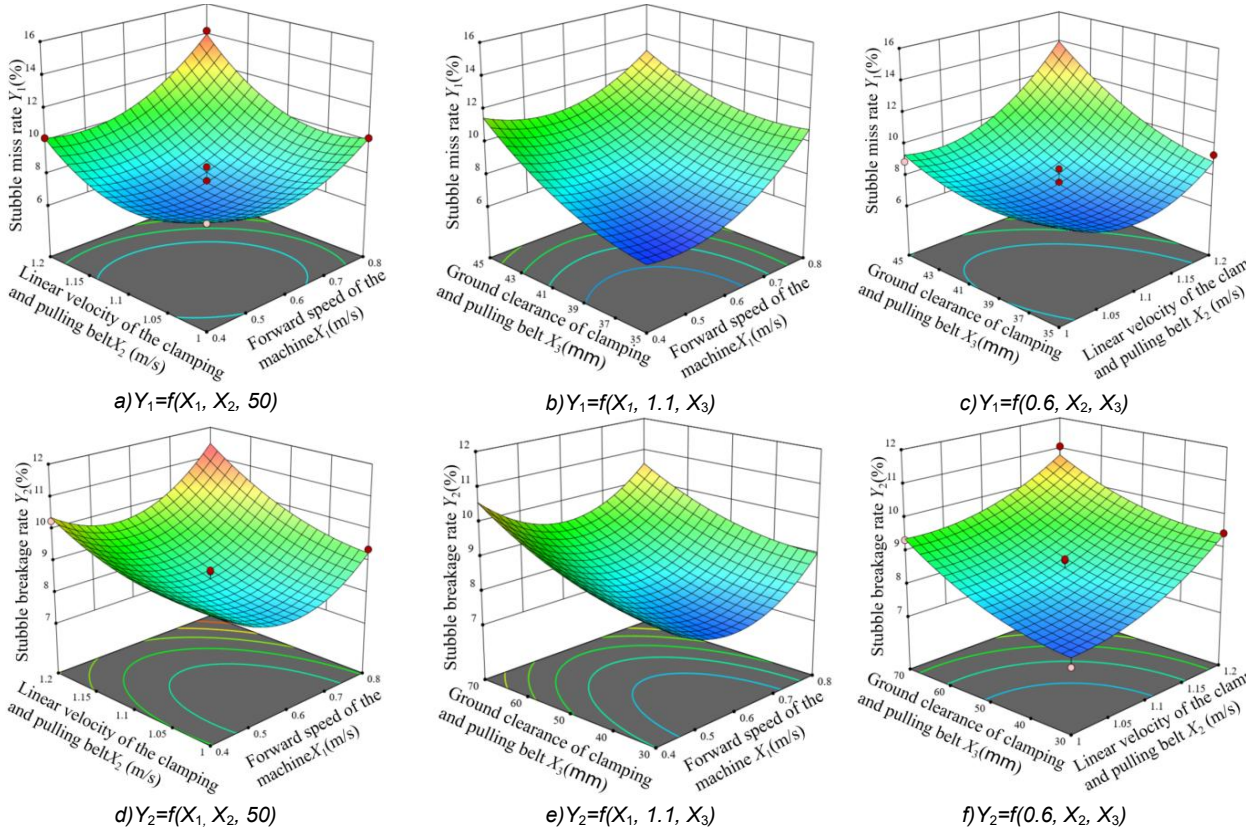

a) $Y_1=f(X_1, X_2, 50)$ b) $Y_1=f(X_1, 1.1, X_3)$ c) $Y_1=f(0.6, X_2, X_3)$

d) $Y_2=f(X_1, X_2, 50)$ e) $Y_2=f(X_1, 1.1, X_3)$ f) $Y_2=f(0.6, X_2, X_3)$

Fig. 11 – The interactive influence of experimental factors on evaluation indicators

To ensure effective stubble clamping and pulling, both the optimization objectives for stubble miss rate Y_1 and stubble breakage rate Y_2 were set to "minimize." Simulation experiments showed that as the height of the CPB above the ground decreases, the clamping point on the stubble lowers, leading to increased soil disturbance. Thus, the optimization objective for the CPB height above the ground was set as "in range" with a preference for the "Lower 50." The optimal parameter combination obtained through optimization was as follows: forward speed of the device at 0.512 m/s, linear speed of the CPB at 1.08 m/s, and CPB height above the ground at 50 mm. This configuration yielded the best clamping and pulling performance, with predicted stubble miss rate at 8.67% and stubble breakage rate at 7.11%.

BENCH TESTING VERIFICATION

Test conditions

To assess the reliability of the belt-clamping potato stubble clamping and pulling device, bench tests were performed under laboratory conditions. The experimental setup is shown in Figure 12, the potato variety used in the tests was “Xisen No.3”. Prior to testing, the potato stubbles were preprocessed in accordance with the technical requirements for potato vine killing, which included removal of leaves and soil from the root zone. The measured stubble parameters were as follows: stem length ranged from 117 mm to 153 mm, stem diameter from 8.72 mm to 12.4 mm, and stem moisture content was approximately 93.2%. The test equipment comprised a belt-type potato stubble clamping and pulling device, an electronic scale, a vernier caliper, a drying oven, and other auxiliary instruments.

Fig. 12 – Experimental test rig of belt-type potato stubble clamping and pulling device

Test methods

Based on the results of simulation tests, the evaluation criterion was the stubble miss rate. Each test group was supplied with 50 stubble plants, and the ratio λ of the CPB operating speed to the device forward speed was 2.1. Three operating conditions were set, low speed (0.4 m/s), medium speed (0.5 m/s), and high speed (0.6 m/s). The stubble miss rate was calculated for each condition, with each condition repeated three times to obtain the average value, the stubble miss rate was calculated using the following equation：

$$Y = \frac{P_1}{P_0} \tag{15}$$

where: Y is the stubble miss rate; P_1 is the number of miss stubble per group; P_0 is the total stubble count per group

Results and analysis

The test results of the stubble clamping and pulling device are presented in Table 6. As shown in the table, the stubble miss rate Y reaches its minimum value at the medium-speed setting, indicating the best clamping and pulling performance of the device. The experimental results under low-, medium-, and high-speed settings are generally consistent with the simulation results, demonstrating that the established discrete element model of the clamped stem segment can be used to simulate the stubble clamping and pulling process and meets the operational requirements for the removal of stubble type residues.

Table 6

Experimental results

Test number	Average number of miss stubble	Average miss rate of stubble Y/%
Low (0.4 m.s^{-1})	5	10
Middle (0.5 m.s^{-1})	3	6
High (0.6 m.s^{-1})	6	12

CONCLUSIONS

A novel belt-type clamping and pulling device was designed for potato stubble removal. Capable of effectively clearing stubble after vine-killing, it facilitates more efficient and higher-quality mechanized harvesting. By implementing flexible clamping and inducing reciprocating oscillation in the stubble during extraction, the process successfully increases the success rate of pulling and minimizes breakage. Based on the analysis of the causes of missed pulling and stubble breakage during the stubble pulling process, three critical parameters influencing operational effectiveness were identified: the forward speed of the device, the linear velocity of the CPB, and the ground clearance of the CPB. Bench tests were conducted, and the results were combined with the analysis in the preceding section to conclude that when the forward speed of the device is 0.512 m/s, the linear velocity of the CPB is 1.08 m/s, and the ground clearance of CPB is 50 mm, the belt-type clamping and pulling device has good pulling performance and anti-blocking performance, meeting the design requirements for stubble clamping and pulling device.

ACKNOWLEDGEMENT

This research was supported by the National Natural Science Foundation of China (52105266); the General Program of Shandong Provincial Natural Science Foundation (ZR2025MS775); the key open scientific research project of the Institute of Modern Agricultural Equipment, Shandong University of Technology (NZY-2025-04); the Youth Innovation Science and Technology Support Program of Shandong Provincial Colleges (2023KJ152).

REFERENCES

[1] Borchard, M. A. (2001). *Apparatus and method for removing plant stalks from a field and shredding the plant stalks*: U.S. Patent No. 6,185,919. America.

[2] Chen, X., Hu, Z., Wang, B., You, Z., Peng, B., Hu, L. (2019). Design and parameter optimization of the vine separation mechanism for a single ridge and single row sweet potato combine harvester (单垄单行甘薯联合收获机薯秧分离机构设计与参数优化). *Transactions of the Chinese Society of Agricultural Engineering*, Vol. 35, pp. 12-21, China.

[3] Chen, L., Zhao, P., Ming, C., Yu, W., Xiang, R., Fan, M., & Long, G. (2024). Responses of carbon and microbial community structure to soil nitrogen status vary between maize and potato residue decomposition. *Agriculture, Ecosystems & Environment*, Vol. 360, China.

[4] Dorokhov, A., Ponomarev, A., Zernov, V., Petukhov, S., Aksenov, A., Sibirev, A., ... & Godyaeva, M. (2022). The results of laboratory studies of the device for evaluation of suitability of potato tubers for mechanized harvesting. *Applied sciences*, Vol. 12, Russia.

[5] Dirr, J., Gebauer, D., & Daub, R. (2023). Localization and grasp planning for bin picking of deformable linear objects. *Procedia CIRP*, Vol. 118, pp. 235-240, Germany.

[6] Gadir, E. A., & Gibreel, T. M. (2013). Development of tractor operated cotton stalk puller. American *Journal of Experimental Agriculture*, Vol. 3, pp. 495-505. Sudan.

[7] Hou, J., Li, C., Lou, W., Li, T., Li, Y., Zhou, K. (2023). Operation Mechanism Analysis and Test of Press Root Cutting Device for Garlic Combine Harvester (大蒜联合收获机浮动式夹持装置设计与试验). *Transactions of the Chinese Society for Agricultural Machinery*, Vol. 54, pp. 137-145, China.

[8] Heltoft, P., Wold, A. B., & Molteberg, E. L. (2016). Effect of ventilation strategy on storage quality indicators of processing potatoes with different maturity levels at harvest. *Postharvest Biology and Technology*, Vol. 117, pp. 21-29, Norway.

[9] Hachiya, M., Amano, T., Yamagta, M., & Kojima, M. (2004). Development and utilization of a new mechanized cabbage harvesting system for large fields. *Japan Agricultural Research Quarterly: JARQ*, Vol. 38, pp. 97-103, China.

[10] He, Y., Xing, W., Wu, M., Quan, W., Chen, C. (2018). Calibration of Discrete Element Parameters for Loamy Soil Based on Piling Experiments (基于堆积试验的壤土离散元参数的标定). *Journal of Hunan Agricultural University*, Vol. 44, pp. 216-220, China.

[11] Kaur, T., Sharma, P. K., Brar, A. S., Vashisht, B. B., & Choudhary, A. K. (2024). Optimizing crop water productivity and delineating root architecture and water balance in cotton–wheat cropping system

through sub-surface drip irrigation and foliar fertilization strategy in an alluvial soil. *Field Crops Research*, Vol. 309, India.

[12] Khamaletdinov, R., Martynov, V., Mudarisov, S., Gabitov, I., Khasanov, E., & Pervushin, A. (2020). Substantiation of rational parameters of the root crops separator with a rotating inner separation surface. *Journal of Agricultural Engineering*, Vol. 51, pp. 15-20, Russia.

[13] Lee, J. Y., Seo, Y. S., Park, C., Koh, J. S., Kim, U., Park, J., ... & Song, S. H. (2020). Shape-adaptive universal soft parallel gripper for delicate grasping using a stiffness-variable composite structure. *IEEE Transactions on Industrial Electronics*, Vol. 68, pp. 12441-12451. China.

[14] Li, Y., Wang, Y., Wang, Y., & Ma, C. (2017). Effects of Vitex negundo root properties on soil resistance caused by pull-out forces at different positions around the stem. *Catena*, Vol. 158, pp. 148-160. China.

[15] Oshunsanya, S. O. (2016). Alternative method of reducing soil loss due to harvesting of sweet potato: A case study of low input agriculture in Nigeria. *Soil and Tillage Research*, Vol. 158, pp. 49-56, Nigeria.

[16] Sun, J., Li, X., Li, S., Wang, X., Wang, L., & Yang, F. (2021). Design optimization and experiment of four-row potato seedling-cutting machine. *Applied Engineering in Agriculture*, Vol. 37, pp. 1155-1167. China.

[17] Wang, H., Zhao, W., Sun, W., Zhang, H., Liu, X., Li, H. (2023). Research progress on mechanized harvesting technology and equipment for potatoes (马铃薯机械化收获技术与装备研究进展). *Transactions of the Chinese Society of Agricultural Engineering*, Vol. 39, pp. 1-22, China.

[18] Wei, Z., Li, H., Su, G., Sun, C., Liu, W., Li, X. (2019). Development of potato harvester with buffer type potato-impurity separation sieve (缓冲筛式薯杂分离马铃薯收获机研制). *Transactions of the Chinese Society of Agricultural Engineering*, Vol. 35, pp. 1-22, China.

[19] Wei, Z., Wang, Y., Su, G., Zhang, X., Wang, X., Cheng, X., Li, X., Jin, C. (2024). Research progress in the technology and equipment for potato mechanized harvesting and impurity removal (马铃薯机械化收获除杂技术与装备研究进展). *Transactions of the Chinese Society of Agricultural Engineering*, Vol. 40, pp. 1-13, China.

[20] Wang Y, Zhao W J, Liu Y D, Chen, Y., & Yang, J. (2021). Simulation of forces acting on the cutter blade surfaces and root system of sugarcane using FEM and SPH coupled method[J]. *Computers and Electronics in Agriculture*, Vol. 180, China.

[21] Wang, Y., Wei, Z., Su, G., Zhang, X., Wang, X., Cheng, X., ... & Jin, C. (2025). Design and study of anti-blocking type potato stubble disc clamping and pulling device based on MBD-DEM coupled simulation. *Computers and Electronics in Agriculture*, Vol. 229, pp. 1-22, China.

[22] Xin, Q., Lü Z., Zhang W., Zhang W., Liu L., Cheng X. (2020). Study on uprooting force of mature potato plants and its influencing factors (成熟期马铃薯秧拔取力及影响因素研究). *Journal of Chinese Agricultural Mechanization*, Vol. 42, pp. 173-176, China.

[23] Yang, R., Yang, H., Shang, S., Xu, P., Cui, G., Liu, L. (2016). Design and Test of Poking Roller Shoving Type Potato Harvester (拨辊推送式马铃薯收获机设计与试验). *Transactions of the Chinese Society for Agricultural Machinery*, Vol. 47, pp. 119-126, China.

[24] Yao, S., Xue, Z., Miao, L. Tan, J., Huang, Y., Zhao, Z. (2023). Development and experiment of the uprooting-type white radish combine harvester (拔取式白萝卜联合收获机研制与试验). *Journal of Chinese Agricultural Mechanization*, Vol. 44, pp. 27-33, China.

[25] Zhao, Q., Wang, J., Wang, Z., Tian, T., Zhao, Y., Cui, L., Hong M. (2020). Application of clamping conveying technology in vegetable harvesting machinery (夹持输送技术在蔬菜收获机械中的应用). *Transactions of the Chinese Society of Agricultural Engineering*, Vol. 10, pp. 8-11, China.

[26] Zou, L., Yuan, J., Liu, X., Li, J., Zhang, P., & Niu, Z. (2021). Burgers viscoelastic model-based variable stiffness design of compliant clamping mechanism for leafy greens harvesting. *Biosystems Engineering*, Vol. 208, pp. 1-15, China.

[27] Zhang, J., Rui, Z., Cai, J., Wang, Y., Yeerbolati·Tiemuer, Gao, Z. (2021). Design and Test of Front Mounted Belt Clamping and Conveying Cotton-stalk Pulling Device (前置式皮带夹持输送棉秆起拔机设计与试验). *Transactions of the Chinese Society for Agricultural Machinery*, Vol. 52, pp. 77-84, China.